Title

Choline-Based Conductive Microgel Bioink for 3D Bioprinting of Cell-Laden Electroconductive Hydrogels

Author

Naghsh-Nilchi, Hamed

Publication Date

2022

Peer reviewed|Thesis/dissertation

UNIVERSITY OF CALIFORNIA

Los Angeles

Choline-Based Conductive Microgel Bioink for 3D Bioprinting of Cell-Laden Electroconductive Hydrogels

A thesis submitted in partial satisfaction of

the requirements for the degree Master of Science in

Bioengineering

by

Hamed Naghsh-Nilchi

2022

ABSTRACT OF THE THESIS

Choline-Based Conductive Microgel Bioink for 3D Bioprinting of Cell-Laden Electroconductive Hydrogels

by

Hamed Naghsh-Nilchi

Master of Science in Bioengineering

University of California, Los Angeles, 2022

Professor Nasim Annabi, Co-Chair

Professor Paul S. Weiss, Co-Chair

Electroactive hydrogels have great potential as a scaffold for tissue engineering. We present the development of choline-based conductive microgels via microfluidics fabrication incorporated in methacrylated gelatin hydrogel backbone, forming a conductive composite hydrogel. The mechanical, swelling, and *in vitro* degradation properties of the conductive composite hydrogel system demonstrate that the backbone polymer characteristics remain unaffected after incorporation of conductive microgels, making this system modular to be used for

engineering different tissue constructs by only tuning the backbone polymer matching the mechanical, swelling, and degradation properties necessary for engineering the target tissue. The conductivity of the resulting composite hydrogel was in the range of electroactive tissue engineering. In addition, the ability of the conductive composite hydrogel to restore electrophysiological communication was confirmed *ex vivo* allowing this system to restore damaged electroconductive tissue. The non-cytotoxicity of the composite hydrogels was also confirmed via *in vitro* studies using rat C2C12 myoblast cells and lung fibroblast cells. The conductive composite hydrogel system was injectable and used as a bioink to print cell-laden scaffold structures with high fidelity and complexity using Freeform Reversible Embedding of Suspended Hydrogels (FRESH) Carbopol support bath supporting cell viability, attachment, and spreading. Lastly, the conductive composite hydrogel showed minimal inflammatory responses *in vivo* when subcutaneously implanted in a rat model. We have shown a novel conductive microgel-based hydrogel that can be used for engineering and regeneration of electroconductive tissue.

The thesis of Hamed Naghsh-Nilchi is approved.

Jun Chen

Paul S. Weiss, Committee Co-Chair

Nasim Annabi, Committee Co-Chair

University of California, Los Angeles

2022

Figure 1: Fabrication and characterization of Bio-IL functionalized fish GelMA microgels. A) Schematic of the fabrication of conductive Bio-IL-Microgels using a microfluidics step emulsifier to form the microgels through a water-in-in oil emulsion, crosslinked via LAP photoinitiator for 4 minutes, then washed and collected. B) Schematic of the synthesis of Bio-IL microgels formed with methacrylated fish GelMA and acrylated Bio-IL crosslinked using LAP photocrosslinker for 4 minutes C) Optical images of microgels in 0 hours, 2 hours, 4 hours, and 24 hours placed in PBS at 37 °C for swelling study and structural integrity test. D) Microgels swelling size over the period of 24 hours. E) Size distribution of microgels over the period of 24 hours swelling. ----------19

Figure 1: Mechanical and physical properties of Bio-IL-Microgel/p-GelMA hydrogels crosslinked with visible light. A) The microgel concentration and packing are depicted for each condition. Red circles are drawn to show a sample of microgel packing in the composite hydrogel system. B) Tensile Moduli and C) Compressive moduli have been determined by varying polymer Bio-IL microgel concentrations. D) Swelling and E) Degradation of the biomaterials. Scale bar: 100 μm. Error bars indicate standard error of the means; asterisks mark significance levels of $p < 0.05$

ACKNOWLEDGEMENT

Firstly, I would like to thank my advisor Prof. Nasim Annabi for her guidance and support and for giving me the opportunity to conduct research under her supervision. I also would like to thank my committee members, Professors Paul S. Weiss and Jun Chen, for providing support and feedback.

Also, I would like to thank the help and support from Dr. Annabi's lab members, Mahsa, for running the *in vivo* animal model studies, and Hossein for running the rheology studies, along with their help and support to finish this project. I would also like to thank Dr. Dino Di Carlo and his lab member Joseph Michael de Rutte, who provided me guidance and the valuable asset of the microfluidics mold that made this work possible.

Finally, I would like to share my love for my family and friends who were always there for me during this journey. My parents and my sister, thank you for your enthusiasm and belief in me. Also, I want to thank my supportive friends who made this chapter of my life enjoyable.

1 Introduction

Organ and tissue transplantation saves and improves millions of lives every year globally; however, there is a considerable shortage of organs in which only 10% of the worldwide's need for organ transplantation is achieved (1). Consequently, there is a need for functional tissue and organ substitutes to restore or improve damaged tissue functions, which led to the birth of tissue engineering. Tissue engineering addresses this need by restoring, supporting, and enhancing tissue functions by developing scaffolds incorporated with cells and biological molecules (2). Living tissues are ubiquitously heterogeneous with hierarchical structures with dynamic cell and extracellular matrix (ECM) interactions acting in concert at different length scales in multifunctional complexity (3). The scaffold should encompass many tissue properties to recapitulate the necessary function and growth, including mechanical and biological cues, which can determine cellular activities such as adhesion, growth, proliferation, and differentiation (4).

Furthermore, many of the tissues in the body have inherent characteristics such as electrical conductivity, which has been shown to affect the function and growth of many tissues such as bone, wound healing, nerve, myocardium, vascular endothelial cells (4). Hence, electrical properties associated with tissues for scaffold development must be appropriately controlled to mimic the natural tissue conductivity. Tissue microenvironment is considerably complex compared to the developed two-dimensional (2D) culture models or even three dimensional (3D) models due to lack of means to construct a living organ model at proper micro and macro scale; hence, 3D bioprinting has gained popularity to make cell-laden scaffolds with designed tissue and organ architectures with great control, flexibility, speed, and precision (5).

Conductivity is an important parameter necessary to mimic the electroactive environment

of many excitable tissues and cells such as the heart, nervous system, skeletal and smooth muscles cells, as well as bone tissues (5). Many biomaterials have been developed to mimic the electrical microenvironment in the native tissues such as electroconductive polymers, including polyaniline (PANI), polypyrrole (PPy), and poly(3,4,-ethylenedioxidythiophene) (PEDOT), and bio ionic liquids or conductive nanomaterials such as graphene, carbon nanotubes (CNTs), and gold nanoparticles (AuNPs) (7). Despite all these strategies, numerous obstacles are associated with the methods as mentioned earlier. Electroconductive polymers such as PANI, PPY, and PEDOT are associated with insufficient biocompatibility as well as poor water solubility, which cannot be well-dispersed and integrated into hydrogels leading to weak mechanical (e.g., brittleness) and conductivity properties (8-10). Graphene and CNTs suffer from low-self healing efficacy, poor mechanical toughness due to weak interactions (hydrogen bonds, host-guest interactions, etc.), and formation of aggregates during hydrogel development (11-13). Moreover, AuNPs are expensive and time-consuming to prepare and are associated with cytotoxicity and genotoxicity caused by suppression of cell growth, generation of reactive oxygen species that can damage proteins, lipids, and DNA, as well as slow rate of body clearance (8, 14-18). We devised an approach to overcome these challenges by embedding microscale conductive building blocks in the form of microgels within a hydrogel matrix.

The development of microgels has been gained attention in a broad range of biomedical applications due to their highly modular capacity to be used as microparticles for therapeutics and drug delivery applications, scaffolds for repair and regeneration of tissues as well as as biological inks (bioinks) for 3D bioprinting (19, 20). Recently, efforts have been made towards developing conductive hydrogels, taking advantage of nanogels and microgels to induce conductivity. For example, Lin *et al.* produced conductive poly (NIPAAm-co-AA) microgels (500-600 nm) by

doping them with PPy (21), Kim *et al*. developed conductive acrylic-based microgels (80–90 nm) by coating them with poly(aniline) and dodecylbenzenesulfonic acid (PANI–DBSA) (22). In another study, Kim *et al*. developed a conductive hydrogel based on acrylic-core microgels (58 nm) coated with PANI, in which the particles were non-aqueous and could not be used to dissolve in biomaterials (aqueous in nature). Zhang *et al*. developed a conductive microgel (~200 nm) based on P(St-NIPAM)/P(NIPAM-co-MAA) coated with AgNPs trapped in PPy, where the conductivity study was inconclusive as they did not perform any experimental validation (23). Hu *et al*. developed conductive microgels based on polystyrene (PS) spheres (5.6 μm) coated with silver to form AgNPs shell. In this work, the PS was removed and only an AgNPs shell remained with 110 nm thickness. There are limitations associate with this method of fabrication including the low affinity of silver coated on PS as well as aggregates of PS/Ag forming due to silver shell irregularities (24). Shang *et al*. developed PNIPAM-co-AAC microgels doped with conductive PEDOT: PSS. This system was both sensitive to pH and temperature changes, which could affect the backbone of the microgels formed based on PNIPAM. As the temperature increased, the microgels shrunk which led to higher conductivity; however, as the pH was changed from 3 to 7, the microgel swelled, leading to a decrease in conductivity (25). Zhao *et al*. developed a supercapacitor stretchable hydrogel based on conductive microgels fabricated using PEDOT and polyacrylamide (PAAm). One downside to use of PEDOT in junction with PAAm was the high viscosity debilitating the polymerization of the microgels leading to a rigid and brittle network as well as decreasing the toughness of the system (26). Feig *et al*. developed an injectable granular conductive system based on fragmented PEDOT: PSS gel. However, their study showed a reduction in cell viability by ~20%. Moreover, the fragmentation resulted in a decrease in the storage modulus compared to the bulk PEDOT: PSS network (27). In most of the studies

abovementioned, since they were not intended for biomedical applications, no biocompatibility study was performed, making the systems inconclusive to be used for biomedical applications. Furthermore, Shin *et al*. developed an injectable and conductive hydrogel based on hyaluronic acid (HA) conjugated with gallol moieties, which act as chelators coupled with silver nanoparticles (AgNPs) leading to the conductivity of the network. The drawbacks associated with this system was the pH dependency of the AgNPs leading to varied size distribution of microgels when chelated to the gallol groups. Also, the spatial distribution and chemical stability of AgNPs can affect the conductivity of the network. The study also showed a drop-in cell viability when compared to the control with no AgNPs. Moreover, the conductivity was dropped by at least 3 folds when the system was placed in an incubator at body temperature for 5 days (28). Despite these recent advances in improving the electrical conductivity performance of the polymers and hydrogels, several limitations associated with the synthesis and delivery of conductive functionality remain. Hence, there exists a need for development of a biocompatible conductive moiety that can be established in biomaterials.

We propose an approach to overcome these challenges by engineering a choline-based conductive microgel system. Choline ((2-hydroxyethyl)trimethylammonium) is a biochemical well characterized due to its existence in abundance in plants, animals, and human tissues as well as a precursor for the neurotransmitter acetylcholine and phospholipids, which are principal elements of biological membranes (28). Choline is a cationic moiety and one of the main components of bio-ionic liquids (Bio-ILs), comprised of naturally-derived components with excellent water solubility, biodegradability, and biocompatibility (29). Ionic liquids (ILs) have many advantageous properties such as low melting points, solvation capabilities, low vapor pressure, and excellent thermal stability, besides their inherent ionic conductivity (30). Hence,

choline-based Bio-IL has gained much interest in developing conductive, adhesive, and hemostatic biomaterials as well as drug delivery systems (6, 29, 31, 32, 33). Another criterion essential to recapitulate the tissue microenvironment is the architecture of the building blocks of cells and tissues structured in the body.

3D bioprinting is an intriguing technique to reproduce identical and complex functional cellular and extracellular components of human tissues and organs (34). This is done through the layer-by-layer deposition of biologically active ingredients such as growth factors, cells, and biomaterials referred to as biological inks (bioinks) that can support the growth of the fabricated tissue (35). The architecture is precisely engineered through a predefined structure design in CAD, and the customized shape or geometry can be achieved through 3D bioprinting, providing fully interconnected porous structures with the perspective of mimicking the native tissue environment (36). Extrusion-based printing is one of the most popular methods of 3D bioprinting where the bioink is loaded in a syringe and deposited in a layer-by-layer manner to create the 3D structure; however, a significant challenge for successful bioprinting is that the printed structures are distorted due to soft and liquid-like nature of the bioinks leading to poor shape fidelity (5, 37, 38). This obstacle has been addressed by the Freeform Reversible Embedding of Suspended Hydrogels (FRESH) technique, where the bioink is deposited into a yield-stress support bath that maintains the bioink in place until it is crosslinked (37, 38). There is a potential for the choline-based conductive microgels to engineer a tunable and highly biocompatible bioink for 3D bioprinting of conductive soft tissues.

In this report, electrically conductive choline-based microgels are prepared using microfluidics to yield a dispersion of conductive microgels in a photocrosslinkable gelatin-based biopolymer. The engineered microgel-based hydrogel was then used as a bioink for 3D printing of

cell-laden structures. We studied the physical properties of the bioink prepared with the conductive microgels. The optimum conductivity condition of the bioink was formulated and revealed to be highly biocompatible in both *in vitro* and *in vivo* studies. The bioprinting was then optimized using the FRESH technique with Carbopol microparticles as the support bath then biocompatibility of the printed structures was validated. We have shown our engineered choline-based conductive microgels has the potential to be used as a conductive bioink for printing complex architectures in applications for electroactive tissue engineering.

2 Materials and Method:

2.1 Materials:

Gelatin derived from porcine skin, gelatin derived from cold-water fish skin, methacrylic anhydride, choline bicarbonate (~80% in H2O), and lithium phenyl-2,4,6-trimethylbenzoylphosphinate (LAP) were all purchased from Sigma-Aldrich. Acrylic acid and ethyl acetate were purchased from Thermo Fisher Scientific. Dialysis tubing (MWCO = 12-14 kDa) was purchased from Spectrum Laboratories. Pico-Surf™ surfactant was purchased from Sphere Fluidics. Novec™ 7500 engineering fluid was purchased from 3M. Tygon Flexible Plastic Tubing (0.02" ID x 0.06" OD) was purchased from Saint-Gobain. SYLGARD™ 184 Silicone Elastomer Kit was purchased from Dow Corning. Aquapel® was purchased from an online store (Amazon). Carbopol ETD 2020 was purchased from Lubrizol. Dulbecco's phosphate-buffered saline (DPBS) was purchased from HyClone. Collagenase type II was purchased from Worthington Biochemical Co. PrestoBlue cell viability reagent, and live/dead viability kits were purchased from Invitrogen. Dulbecco's Modified Eagle Medium (DMEM), Fetal Bovine Serum (FBS), and Penicillin–Streptomycin (Pen-Strep) were purchased from Gibco.

2.2 Synthesis of bio-IL:

Bio-IL synthesis was performed as described previously (29). Briefly, Bio-IL synthesis was performed by reacting 16.5 g of choline bicarbonate with 7.2 mL of acrylic acid for 5 hours under continuous stirring (120 rpm) at 55 °C. The reaction was then halted, and the solution was transferred to a falcon tube. Then equal parts of ethyl acetate were added to the solution and were mixed vigorously for 15 minutes. We then observed two phases forming (visible by the naked eye). The top phase was the ethyl acetate and the unreacted acrylic acid, which was discarded. The bottom phase was recovered as the Bio-IL solution formed. The process was repeated 3 times to

make sure there is no unreacted acrylic acid present.

2.3 Synthesis of gelatin methacryloyl (GelMA):

GelMA synthesis was performed as described previously (39). Briefly, 10 wt% gelatin was dissolved in Dulbecco's phosphate-buffered saline (DPBS; GIBCO) by stirring at 60 °C for 4 hours. Then, methacrylic anhydride (MA) (Sigma-Aldrich) was added dropwise to the solution and reacted for 3 hours at 60 °C. The reaction was stopped by diluting the reactants with the addition of DPBS (5x). The reaction mixture was then dialyzed against deionized water through a dialysis tubing (12-14 kDa molecular weight cutoff) for 7 days to remove the unreacted MA altogether. The final solution was finally lyophilized and stored at 4 °C.

2.4 Microfluidics Polydimethylsiloxane (PDMS) step-emulsifier fabrication:

The step-emulsifier devices were fabricated using soft lithography from a mold provided by the Di Carlo lab at UCLA using two-layer lithography with channel orifice of 200 μm and oil reservoir height of 65 μm. The microfluidic step-emulsifiers were molded from the masters provided using PDMS SYLGARD™ 184 Silicone Elastomer Kit (Dow Corning) where the base and curing agent were mixed at 10:1 mass ratio and poured over the master mold, degassed then cured at 50 °C overnight. The PDMS devices were peeled from the mold then inlets and outlets of the microfluidics device were punched with 0.8 mm holes. Then the PDMS device and microscope glass slides were oxygen plasma treated for 60 seconds and bonded together to enclose the microchannels. In the end, the devices were Aquapel® treated for <60 seconds and washed with Novec™ 7500 oil to ensure the microchannels were flourophobic. The devices were then placed in an oven at 50 °C for <1 hour to ensure the residual Novec™ 7500 oil was fully evaporated (40).

2.5 Fabrication of conductive choline-based fish GelMA microgels:

15 wt% fish GelMA and 0.4 wt% lithium phenyl-2,4,6-trimethylbenzoylphosphinate (LAP) (Sigma-Aldrich) photoinitiator were dissolved in a Bio-IL solution for ~ 1h at 50 °C to prepare the aqueous solution of the microfluidics device. The dispersed phase (oil phase) of the microfluidic device was prepared by making a mixture of 0.5 wt% Pico-Surf™ (Sphere Fluidics) surfactant in Novec™ 7500 (3M) oil. The solutions were injected into the step-emulsifier microfluidics device using syringe pumps to form stabilized fish GelMA/Bio-IL microgels. The GelMA-Bio-IL phase was pumped at 5 µL/min, and the oil phase was pumped at 200 µL/min. The microgel suspension was then photocrosslinked using visible light by running the particles continuously through a Tygon Flexible Plastic Tubing 0.02" ID x 0.06" OD (Saint-Gobain) with a light-emitting diode (LED) light (405 nm, 10W) for 3 minutes then collected in Eppendorf tubes for post-processing. The crosslinked fish GelMA conjugated Bio-IL microgels are extracted from the Novec™ 7500 oil solution by adding hexane to lower the oil density three times, then washing the microgels with DPBS three times to ensure the remaining oil is washed away (40). The fish GelMA conjugated Bio-IL microgels are then washed with pure ethanol 3 times and placed at 4°C overnight for sterilization.

2.6 Conductive choline microgel encapsulated composite hydrogel preparation:

The composite hydrogel with bio-IL microgels was prepared by dispensing microgels at 0, 10, 20, 30, 40, and 50 wt% in 10 wt% porcine GelMA (p-GelMA) containing 0.05 wt% LAP photoinitiator and mixed homogenously and placed in a 37 °C oven. The solution was then casted in a PDMS mold (10 mm L × 5 mm W × 1 mm H) and crosslinked for 4 minutes using a light-emitting diode (LED) light (405 nm, 10W).

2.7 Preparation of the Carbopol support bath:

Carbopol was prepared as described with some modifications (41). In brief, 1.8 wt% of Carbopol ETD 2020 (Lubrizol) was dissolved in 25 mL DPBS and vortexed. Then, 550 µL of 10 M NaOH was added to the 25 mL Carbopol solution and vortexed vigorously until a slurry gel was obtained. Next, the solution was centrifuged at 4000 × g for 10 minutes until the gel became homogeneously dispersed. The homogeneous Carbopol gel was sterilized under a high-intensity UV source for 10 minutes then kept in a 4 °C fridge for storage.

2.8 Conductive choline-based fish GelMA microgel characterization:

The swelling study of fish GelMA-Bio-IL microgels was determined by placing microgels in DPBS at 37 °C and imaging them to determine their sizes over different time intervals for 48 hours. The microgel dimensions were measured using a custom MATLAB code developed to measure and assess their sizes unbiased.

2.9 Preparation of the Carbopol support bath:

Carbopol was prepared as described with some modifications (41). In brief, 1.8 wt% of Carbopol ETD 2020 (Lubrizol) was dissolved in 25 mL DPBS and vortexed. Then, 550 µL of 10 M NaOH was added to the 25 mL Carbopol solution and vortexed vigorously until a slurry gel was obtained. Next, the solution was centrifuged at 4000 × g for 10 minutes until the gel became homogeneously dispersed. The homogeneous Carbopol gel was sterilized under a high-intensity UV source for 10 minutes then kept in a 4 °C fridge for storage.

2.10 Conductivity characterization:

Conductive hydrogel with varying Bio-IL microgel concentrations (e.g., 0, 10, 20, 30, 40,

and 50 wt%) was prepared as explained above. A two-probe measuring setup using a potentiostat model 263 A, AMETEK® was used to measure the conductivity of the prepared Bio-IL microgel laden porcine GelMA hydrogels. The hydrogel samples were placed between two copper sheets coated with silver paste and voltage was applied in 0.05 V increments from -1 to 1 V. The current versus voltage variations was recorded; hence, the resistance was measured, and the conductivity (κ, S/cm) was calculated using the following equation:

$$\kappa = \frac{I}{V} . \frac{L}{A}$$

where V was the measured voltage, with the current provided by the potentiostat, A (cm^2) was the cross-section area of the hydrogel sample, and L (cm) was the distance between the two probes attached to the ends of the hydrogel sample.

2.11 Mechanical characterization:

Mechanical properties of the hydrogels were evaluated using a mechanical testing machine, Instron 5943 equipped with a 100 N load cell. Both the tensile and compression studies were analyzed for each of the hydrogels with varying microgel concentrations. The hydrogels were prepared in a cuboid PDMS mold (10 mm L × 5 mm W × 1 mm H) and in cylindrical PDMS mold (5 mm D × 5mm H) for tensile and compression studies, respectively. The tensile and compression studies were performed at a constant strain rate of 1 mm/min, and data was recorded using Bluehill 3 Universal software. The hydrogels were held between two tensile grips and elongated until failure for the tensile studies. The elastic modulus was determined by taking the tangent slope of the stress-strain curve, and the toughness was measured calculating the area under the stress-strain curve, and stretchability was determined at the maximum strain value where the hydrogel failed. For the compression studies, the hydrogels were placed and held between two compression plates

and compressed until failure. The compression modulus was determined by taking the tangent slope of the stress-strain curve between 0 to 10% of the compressive strain of the hydrogels, and the toughness was measured by calculating the area under the stress-strain curve. At least 3 samples were tested for each condition to obtain the average and standard deviation.

2.12 Swelling ratio and water uptake characterization:

compression studies. Then the samples were lyophilized to remove the water then their dry weights were recorded. Then the samples were placed in DBPS in an oven at 37 °C and reweighted at prearranged timepoints (1,4, 12, 24, 120 hours). The swelling ratio and water uptake capacity was evaluated using the following equation below:

$$\text{Swelling ratio (\%)} = \frac{w - wo}{wo}$$

where w_o is the initial dry weight of the sample, and w is the dry weight after time t.

2.13 *In vitro* degradation characterization:

Hydrogels samples were fabricated using cylindrical PDMS molds previously explained for the compression studies. Then the samples were lyophilized to remove the water. Their dry weights were recorded. Then the samples were placed in DBPS (1X) supplemented with 20 µg/ml collagenase type II enzyme at 37 °C oven continuously for 14 days. The DBPS – collagenase type II solutions were substituted every 2 days to maintain constant proteolysis activity. At the prearranged time points (days 1,4,7, and 14), the samples were removed, lyophilized for 24 hours, and weight measurements were performed. The weight remaining percentage was calculated using the equation below:

$$\text{Weight remaining (\%)} = \frac{w}{wo}$$

where w_o is the initial dry weight of the sample, and w is the dry weight after time t.

2.14 Rheology characterization:

A rheometer (MCR 302, Anton Paar) equipped with parallel plates with a gap size of 1 mm and a diameter of 8 mm was used to characterize the rheological properties of GelMA prepolymer and microgel (50 wt%)-laden-GelMA prepolymer. The solutions were prepared and pipetted onto the rheometer then the excess solution was trimmed with a spatula before measurements. The polymer solutions were prepared as outlined before and pipetted onto the rheometer. Any excess solution was removed with a spatula before these measurements. The viscosity of the hydrogel samples was measured as a function of temperature with a shear rate at 50 s^{-1} and the temperature sweep rate of 2 °C min^{-1}. Storage modulus (G') and loss modulus (G") of the hydrogel samples were recorded in a temperature sweep test starting from 50 °C to 10 °C at a rate of 1 °C/min followed by a 3 min isothermal period and then a heating cycle over the same temperature range. The storage (G') and loss modulus (G") values were recorded at 10% strain and 1 Hz oscillation.

2.15 *In vitro* biocompatibility characterization:

The *in vitro* biocompatibility of the Bio-IL microgels was assessed using lung fibroblast cells and C2C12 myoblast cells. Live/Dead staining kit was used to analyze the cellular spreading and viability, as well as PrestoBlue cell viability reagent to analyze the metabolic activity of the cells. Hydrogel samples were formed by the addition of a 10 µL hydrogel precursor at a spacer with 120 µm height. Then a TMSPMA-coated glass slide was placed on top of the hydrogel precursor on the spacer and photocrosslinked for 20 seconds using visible light. For 2D cell culture studies, the cells were then seeded on the surface of the hydrogel with a seeding density of 2×10^4 cells/cm^2, and then the cell seeded hydrogels were placed in 24-well plates containing 1 mL of growth medium (DMEM) supplemented with 10% FBS and 1% Pen-Strep. For the 3D cell

culture studies, the hydrogel precursor was mixed with cells at 5×10^5 cells/mL, then added at a spacer and photocrosslinked. The cell-laden hydrogels were washed with the growth medium (DMEM) then placed in 24-well plates containing 1 mL of growth medium (DMEM) supplemented with 10% FBS and 1% Pen-Strep. All samples were incubated at 37 °C in a humidified atmosphere with 5% CO_2 for the duration of the studies, and the complete growth medium was refreshed every 2 days.

The cell viability and spreading were assessed through a live/dead stain kit according to the manufacturer's instructions. In brief, samples were stained with 0.5 μL/mL of calcein-AM and 2.0 μL/mL of ethidium homodimer-1 (EthD-1) in DPBS and incubated for 30 minutes at 37°C in a 5% CO_2 humidified incubator. Fluorescent imaging was performed using the Zeiss Axio Observer Z1 inverted microscope at days 1,3, and 5 post-seeding, and evaluation and analysis were performed through the ImageJ software. The cell viability analysis was based on the ratio of the number of live cells to the total number of cells. Furthermore, the metabolic activity of cells was evaluated at days 1, 3, and 5 post-seeding using the commercially available PrestoBlue assay according to the manufacturer's instructions. In brief, samples were incubated in 10% PrestoBlue in growth medium (DMEM) supplemented with 10% FBS and 1% Pen-Strep for 40 minutes at 37 °C in a 5% CO_2 humidified incubator. The fluorescence intensity of the PrestoBlue was determined using a Synergy HT plate reader (BioTek) at excitation/emission: 535/590 nm. For all the studies, there were at least 4 samples to ensure statistical significance.

2.16 3D bioprinting optimization using conductive bioink:

Cell-laden and acellular bioink (50 wt% microgel content) were prepared and loaded into a 5 mL syringe affixed with a 25-gauge blunt needle. The Carbopol slurry gel support bath was prepared as described before and poured into 12 well-plates, and sterilized under a high-intensity

UV chamber. The syringe was then loaded onto an Allevi 3 bioprinter maintained at 30 °C. For the optimization studies, the pressure (5-6 psi) and speed (5-20 mm/s) of the nozzle head holding the syringe were varied for adjusting the flowrate of the bioink being printed into the Carbopol support bath. The printed structures were then photopolymerized through exposure to a light-emitting diode (LED) light (405 nm, 10W) for 2 minutes. The Carbopol support bath was then washed with warm DPBS and DMEM multiple times until the structure was entirely free from the support bath. The bioink was loaded with 5×10^6 cells/mL into the syringe for bioprinting the cell-laden structures. After the Carbopol bath had been removed, the structure was immersed into a growth medium with 10% FBS and 1% Pen-Strep. The medium was changed after 30 minutes to remove the unreacted photoinitiator and placed back in the incubator for the post cell analysis.

2.17 *In vivo* biocompatibility and biodegradation characterization:

The animal protocol was approved by the ICAUC (ARC-2021-113) at the University of California, Los Angeles. Male Wistar rats (~250 g) were purchased from Charles River Laboratories (Boston, MA, USA). Subcutaneous implantation of hydrogels in rats was performed as described previously (42). Briefly, anesthetics were applied by inhalation of isoflurane (~2%), then eight incisions by the size of 1 cm were applied on the rat's dorsal skin. Then, subcutaneous pockets were made using a blunt scissor for hydrogel implantation. Printed and cylindrical samples of 50 wt% microgels encapsulated GelMA and GelMA (control) were implanted in the subcutaneous pockets. The lyophilized hydrogel samples were sterilized using a high-intensity UV light for 10 minutes prior to implantation. After the samples were implanted, the incisions were closed with a 4-0 polypropylene sutures (Ad Surgical). At days 7 ad 28 post-surgery, the rats were euthanized, and hydrogel samples were extracted with surrounding tissues and no surrounding tissues for histological analysis and degradation rates, respectively. Histological analysis was

implemented on the explanted hydrogels with surrounding tissue to evaluate the inflammatory response. Proceeding with the explanted hydrogels, they were fixed in 4% paraformaldehyde for 4 hours, and incubated at 4 °C in sucrose solution at 15 wt% followed by sucrose solution at 30 wt%. Then the samples were immersed in Optimal Cutting Temperature (O.C.T) compound, frozen in liquid nitrogen, and sectioned in slices of 8-10 µm using Leica CM1950 cryostat machine. The slices were mounted on a positively charged sliced using the DPX mountant (Sigma) for hematoxylin and eosin (H&E) staining and ProLongTM Gold antifade reagent (Thermo fisher scientific) for immunofluorescence (IF) staining. H&E staining (Sigma) was performed according to the manufacturer's instructions. Additionally, IF staining was performed on the mounted slices as reported previously. Anti-CD68 (ab125212) (Abcam) was used as primary antibodies and an Alexa Flour 594 conjugated secondary antibody (Invitrogen) as the detection reagent. All the section slides were then counterstained with DAPI (Invitrogen) and visualized using fluorescent imaging with the ZEISS Axio Observer Z7 inverted microscope.

2.18 Statistical Analysis:

Statistical analysis was performed using GraphPad Prism 8. All the data presented are mean +/- standard deviation. A comparison of values was performed using a one-way analysis of variance (ANOVA) and Tukey post-hoc test. Statistically significant values are presented as *$p < 0.05$, **$p < 0.01$, ***$p < 0.001$ and ****$p < 0.0001$.

3 Results and Discussion:

3.1 Fabrication and synthesis of the conductive microgels:

Hydrogel-based microgels have been used in broad range of applications from therapeutics and drug delivery to scaffold development used in the repair and regeneration of tissue as well as development of bioinks for 3D bioprinting (19, 20). Diverse fabrication methods have been used to fabricate microgels including batch emulsions (44), lithography (45), electrodynamic spraying (46), mechanical fragmentation (47) and microfluidics emulsions (48). Batch emulsion is the most convenient method of fabricating microgels with the advantage in its simplicity and high production rate; however, the microgel polydispersity is high and there is a batch-to-batch variation that can affect the microgel's properties (19). Microgels fabricated through lithography method is through photopolymerization where a template is used to imprint the microgels. Using this method, different microgel geometries with monodisperse sizes can be fabricated; however, removing the microgels from the mold is a major constraint along with its low throughput (19). Electrodynamic spraying also has the limitation to produce monodisperse microgel populations (19). Mechanical fragmentation, breaking bulk gel to small pieces, is simple yet very difficult to control the microgel size population (19).

Microfluidics devices have been developed and widely adapted to overcome the polydispersity limitation and to provide precise control over fabrication of microgels. However, one of the major limitations associated with this method is its low throughput (19, 47). Hence, high throughput microfluidics devices have been developed to overcome the throughput challenge (41, 49). In this work, we adopted a step-emulsifier microfluidics droplet generator to achieve high throughput microgel fabrication where the hydrogel precursor (fish GelMA, Bio-IL, and LAP) is injected into parallelized step emulsification microfluidics device at room temperature and

crosslinked downstream of the device using a light-emitting diode (LED) light (405 nm, 10W) for 4 minutes. The crosslinked microgels were then washed with hexane and PBS, and centrifuged to separate the microgels (Figure 1.a). Gelatin derived from fish was used as the microgel backbone as fish gelatin is biocompatible and biodegradable with abundant arginine-glycine-aspartic acid (RGD) sequences that can support cell adhesion (50). Furthermore, fish derived gelatin has a low melting temperature of 10 °C making it in a liquid form at room temperature as well as it has low viscosity, making it a great candidate to be used for microgel production using microfluidics (51). The fish gelatin was modified with methacrylic anhydrate to synthesize fish gelatin methacryloyl (fish GelMA) that is photocrosslinkable in presence of a photoinitiator such as LAP (50). Recently, our group has developed an acrylated choline based Bio-IL that can be conjugated to GelMA via photopolymerization (30), so we took advantage of the acrylated choline and used it as the precursor of the microgel to form the choline based microgel using LAP photocrosslinker (Figure 1.b).

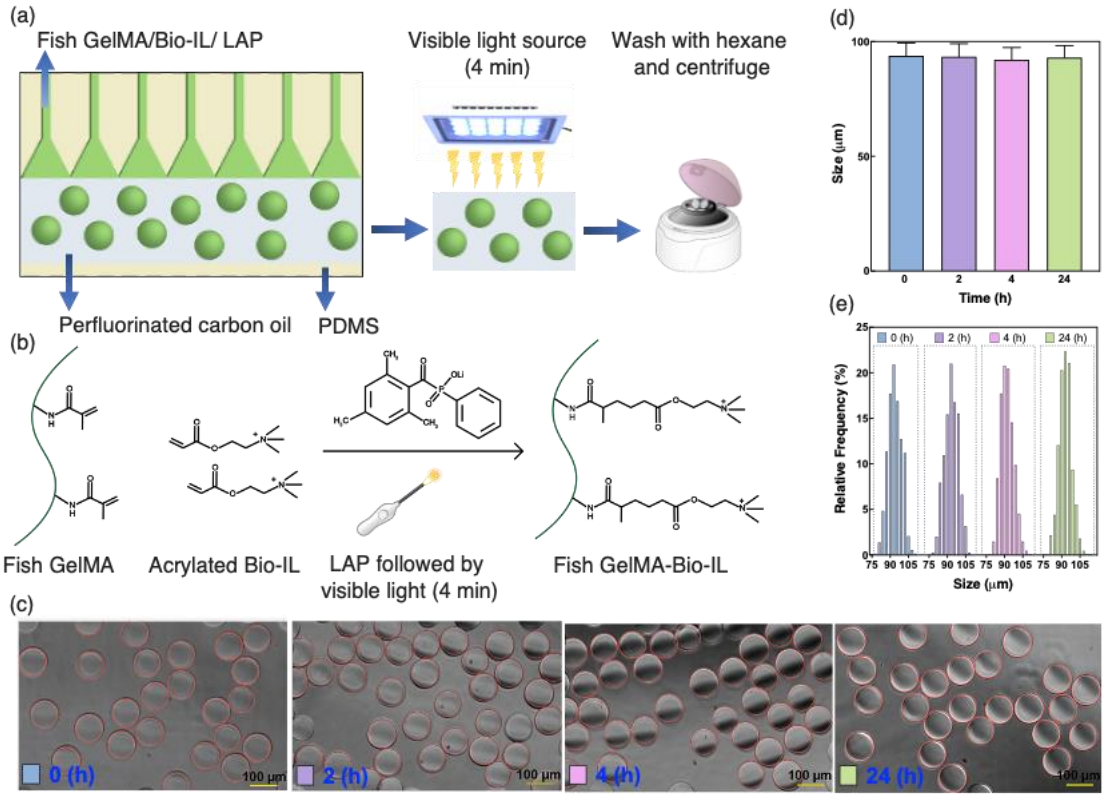

Figure 1: Fabrication and characterization of Bio-IL functionalized fish GelMA microgels. A) Schematic of the fabrication of conductive Bio-IL-Microgels using a microfluidics stepemulsifier to form the microgels through a water-in-in oil emulsion, crosslinked via LAP photocrosslinker for 4 minutes, then washed and collected. B) Schematic of the synthesis of Bio-IL microgels formed with fish GelMA and acrylated Bio-IL and crosslinked using LAP photocrosslinker for 4 minutes C) Optical images of microgels after 0, 2, 4, and 24 hours placed in PBS at 37 °C for swelling study and structural integrity test. D) Microgels swelling size over the period of 24 hours. E) Size distribution of microgels over the period of 24 hours swelling.

We could robustly produce uniform microgels and studied the size and distribution uniformity over the period of 24 hours (Figure 1.c). One of the advantages of the microgels compared to other systems as shown in Fig 1.c is that they were easily separable with no

agglomerates formed as monitored and verified using optical microscopy. The swelling and stability of the microgels over the period of 24 hours of incubation at 37 °C (body temperature) were confirmed with the average diameter size microgels of 93.1 ± 5.44 µm (Figure 1.d) with a highly monodisperse size distribution (Figure 1.e). The results indicate that the microgels had no sensitivity to temperature and swelling as their sizes did not change significantly over the period of 24 hour, making them highly stable and modular to be incorporated in any polymer backbone. Finally, the fabricated choline based microgels were stored in DPBS with 70% ethanol at 4°C overnight prior to mixing the hydrogel prepolymer and characterizations. The engineered conductive microgel developed in this study were highly stable in body temperature conditions and had the advantage of being washed prior to the addition to the biopolymer backbone.

3.2 Characterization of the mechanical properties of the engineered conductive hydrogel:

Making a biomimetic conductive hydrogel for biomedical applications must provide adequate mechanical properties to support cell growth and tissue formation. It has been shown that mechanical forces can affect the tissue development and key cellular functions such as proliferation, differentiation, migration and apoptosis (52). It has been also shown that microgels provide a great degree of tunability and can mimic the soft components of the natural ECM with respect to the backbone structure and mechanical properties (3). In this respect, we have characterized the mechanical properties of the composite choline-based microgels encapsulated in porcine GelMA backbone hydrogel. The mechanical and physical properties of the composite hydrogel (10 wt%) was evaluated at different microgel concentrations (0, 10, 20, 30, 40, and 50 wt%) (Figure 2.a). Tensile and compression tests were performed to evaluate the performance of the porcine GelMA backbone with varying microgel concentrations.

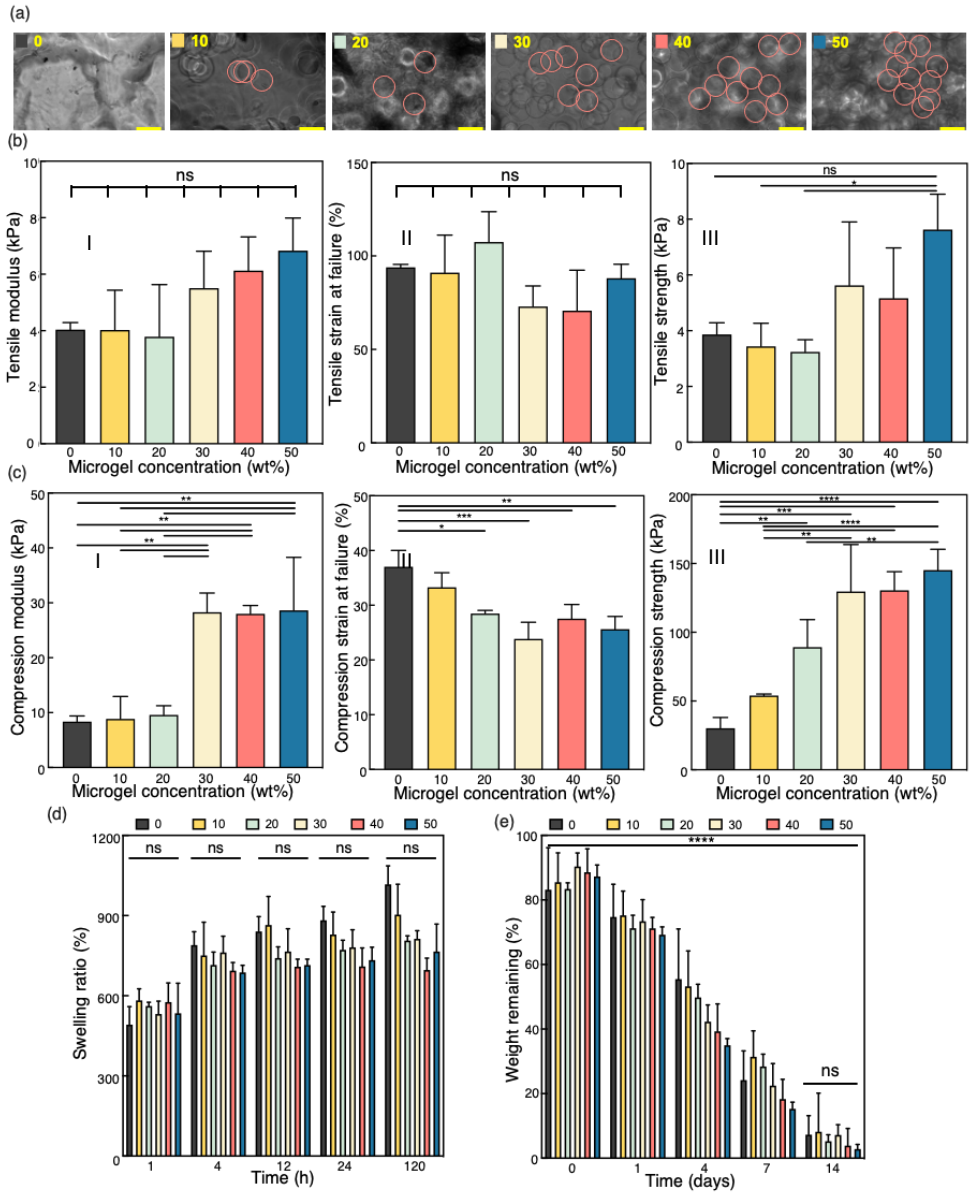

Figure 2: Physical properties of Bio-IL-Microgel/p-GelMA hydrogels crosslinked with visible light. A) Representative microscopic images from hydrogel containing various concentrations of microgels. Red circles are drawn to show a sample of microgel packing in the composite hydrogel system. B) Tensile studies; I) Tensile modulus, II) Tensile strain at failure, and III) tensile strength, and C) Compressive studies; I) Compression modulus, II) Compression strain at failure, and III) Compression strength, all have been determined by varying polymer conductive microgel concentration. D) Swelling and E) Degradation of the biomaterials. Scale bar: 100 µm. Error bars

indicate standard error of the means, asterisks mark significance levels of $p < 0.05$ (*), $p < 0.01$ (**), $p < 0.001$ (***), and $p < 0.0001$ (****).

The tensile results exhibited no significant change in the modulus, elongation, and tensile strength of the hydrogels formed with varying microgel concentrations (Figure 2.b). The tensile modulus ranges from ~4.04 to 7 kPa by varying the microgel concentrations, specifically, at the 0 wt% microgel concentrations, the tensile modulus is at 4.04 ± 0.25 kPa and at the 50 wt% microgel concentration, the modulus is at 6.83 ± 1.12 kPa (Figure 2.b.I). The tensile strain at failure with varying microgel concentrations ranges in the ~90% where at the 0 wt% microgel concentrations, the hydrogel elongated 93.9 ± 1.75 % and at 50 wt% microgel concentration elongated for 88.11 ± 7.43 % (Figure 2.b.II). The tensile strength ranged from ~3.87 to 7.63 kPa with the 0 wt% microgel concentration was at 3.87 ± 0.42 kPa and the 50 wt% microgel concentration at 7.63± 1.27 kPa (Figure 2.b.III).

On the other hand, the compression modulus of hydrogel formed with microgel concentration above 30 wt% significantly increased. The compression modulus for the 0 wt%, 10wt%, and 20 wt% were 8.36 ± 1.03 kPa, 8.85 ± 4.09 kPa, and 9.58 ± 1.66 kPa, respectively (Figure 2.c.I). The compression modulus at 30 wt% towards 50 wt% increased at least by 3 folds to 28.29 ± 3.48 kPa for the 30 wt% microgel concentration, 27.99 ± 1.51 kPa for the 40 wt% microgel concentration, and 28.63 ± 9.65 kPa for the 50 wt% microgel concentration. The compression strain at failure decreased from ~40% to ~30% for the 0 wt% and 50 wt%, respectively (Figure 2.c.II). The compression strength for the 0 wt% microgel concentration was 30.22 ± 7.81 kPa and for the 50 wt% microgel concentration was at 143.24 ± 15.13 kPa (Figure 2.c.III), which could be due to higher microgel concentrations leading to a densely packed composition with a high-volume fraction shown in Fig 2.a. At higher microgel densities, as the

hydrogel compositions were compressed, the microgels started to exert more force since the microgel polymer concentration was at 15 wt% compared to the backbone porcine GelMA of 10 wt%. The compression strain at its failure ranged from ~37% to 26 % where the failure for the 0 wt% microgel concentrations was measured to be at 37.04 ± 2.98 % and for the 50 wt% microgel concentration was measured to be 25.62 ± 2.33 % (Figure 2.c.III). The densely packed composition of the microgels although crosslinked to the backbone polymer had lower crosslinking; hence, making the backbone hydrogel break since the pressure on the crosslinked microgels increased breaking the bonds.

Furthermore, excessive water uptake and swelling as well as degradation can impair mechanical properties and time necessarily needed for tissue growth in hydrogels. Hence, we evaluated the water uptake and swelling ability along with the in vitro degradation of the composite porcine GelMA encapsulated with microgels at aforementioned concentrations. The results demonstrated that maximum swelling and water uptake was achieved after 4 hours with no significant change in microgel concentrations compared to porcine gelatin itself (Figure 2.d). The maximum swelling ratio for the 0 wt% microgel concentration was 1016.98 ± 68.98 % and for the 50 wt% microgel concentration was 768.63 ± 102.41 %, showing the ability of the composite structure to swell that is advantages for cell growth and proliferation.

Lastly, the in vitro degradation of the composite hydrogel was characterized for 14 days (Figure 2.e). Biodegradation is one of the key properties of biomaterial design for tissue engineering (53), and our results indicated that the composite hydrogels degraded ~80% after 14 days incubation in nm enzyme solution and the microgels incorporated in the composite hydrogel did not significantly change the degradation profile of the composite hydrogel. Altogether, our results demonstrate the mechanical properties and the physical properties (i.e., swelling,

degradation) of the composite hydrogel did not vary due to the addition of conductive microgels. These results suggest there should be available methacrylate functional groups crosslinking sites available on the microgels leading to conjugation with the bulk GelMA, so they can be integrated in the composite system. The engineered conductive microgel has the advantage to be incorporated in photocrosslinkable biomaterials without compromising the backbone mechanical, swelling and degradation properties.

3.3 Characterization of the electroconductive properties of the engineered conductive hydrogel:

The electrical conductivity in tissue regeneration has been shown to improve bone formation, wound healing, never, myocardium, and vascular endothelial cell functions (4). Conventional techniques used for the development of conductive hydrogels exhibit many limitations associated with cytotoxicity, biodegradation, as well as poor solubility and processibility (7). There has been a development to use Bio-ILs as a new methodology to induce conductivity in hydrogels. Recently, bio-ILs have represented a great opportunity to be used to induce conductivity for biomedical applications due to their wide electrochemical window (53). Many groups have taken advantage of the ionic conductivity associated with ionic liquids where IL's monomers were incorporated in a backbone polymer system to improve the conductivity. Liang *et al.* used 1-butyl-3-methylimidazolium chloride (BMIMCl) IL (54) included in microcrystalline cellulose and PPy as polymers, Robinson *et al.* used 1-decyl-3-methylimidazolium chloride IL (55) to 3D print a sensing skin, and Lu *et al.* used choline based IL (56) as a secondary doping effect in conjunction with PDOT: PSS to induce and improve conductivity. Recently, our group has established a choline-based Bio-IL conjugated to hydrogel networks for the development of conductive hydrogels for cardiac tissue engineering (6, 29). The

Bio-IL developed by our team was synthesized through a reaction of choline bicarbonate and acrylic acid, resulting in a photocrosslinkable choline-acrylate(29). The synthesized choline acrylate monomer solution was mixed with natural (GelMA) and synthetic polyethylene glycol diacrylate (PEGDA) polymers along with photoinitiators Eosin Y, vinyl caprolactone, and triethanolamine, which through photopolymerization the Bio-IL was conjugated to the hydrogel backbone through exposure to visible light. To achieve a cell-compatible composite hydrogel, 15 wt% GelMA with 50/50 GelMA/choline-acrylate ratio was used corresponding to $3.03 \times 10^{-05} \pm 0.72 \times 10^{-05}$ S/m. In this work, we took advantage of this novel synthesized choline-acrylate Bio-IL to fabricate conductive microgels with uniform sizes (Figure 1.d).

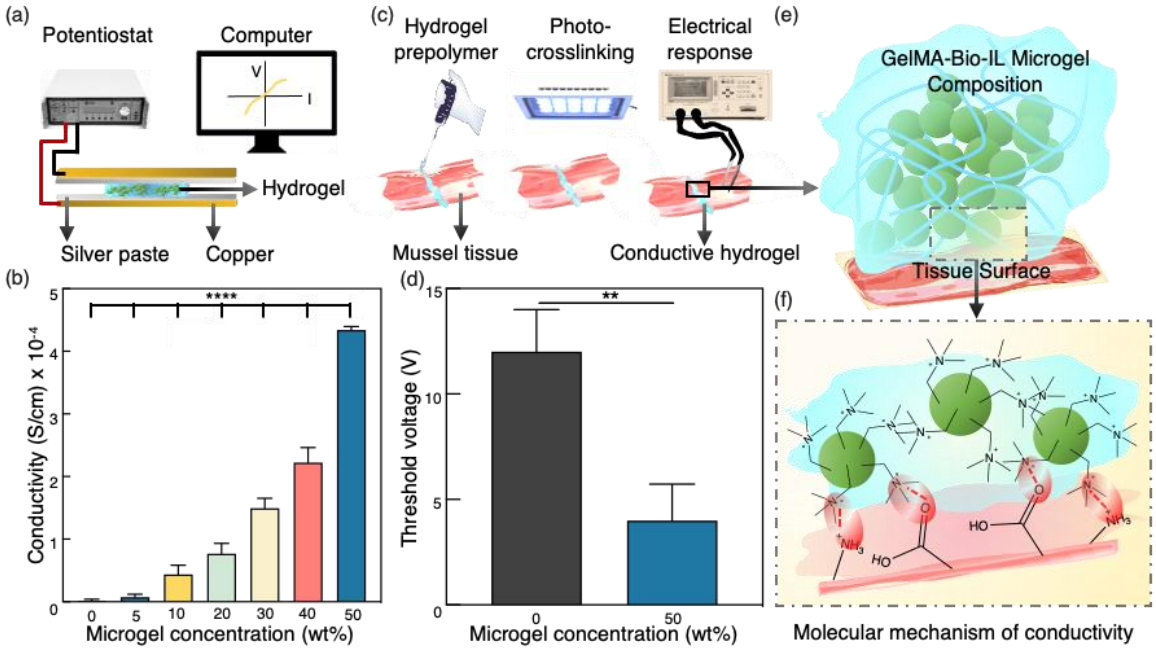

Figure 3: Electrical conductivity of the choline-microgels encapsulated in 10 wt% GelMA hydrogels. A) Schematic of 2 probe conduction test to evaluate the conductivity of the composite hydrogels at different conducive microgel concentrations in 10 wt% GelMA sandwiched in between a copper tape smeared with silver paste. B) Electrical conductivity of Bio-IL-Microgel/p-

GelMA hydrogels at different microgel concentrations. C) Schematic of ex vivo electrical tissue conduction test using isolated abdominal muscle tissues and 50 wt% conductive microgel concentration in 10 wt% GelMA sandwiched in between. D) Threshold voltages at which contraction was achieved on the 50 wt% conductive microgel concentration in 10 wt% GelMA and the GelMA as the control hydrogel. E, F) Molecular mechanism of the conductive tissue stimulation achieved by the conductive microgels. Error bars indicate standard error of the means, and asterisks mark significance levels of $p < 0.05$ (*), $p < 0.01$ (**), $p < 0.001$ (***), and $p < 0.0001$ (****).

Briefly, the conductive microgels were mixed with 10 wt% porcine GelMA to form conductive composite hydrogels at different microgel concentrations (0, 5, 10, 20, 30, 40, and 50 wt%). The composite hydrogels were sandwiched in a copper tape coated with silver paste connected to a two-probe electrical system to measure the change of the current vs. the voltage and calculating the conductivity using Ohm's law (Figure 3.a). We demonstrated incorporation of different microgel concentrations enabled modulation of the electrical properties of the GelMA/microgel composite hydrogel. The conductivity of the 50 wt% increased more than 200-folds from $0.021\times 10^{-04} \pm 0.012 \times 10^{-04}$ S/cm (0 wt%) to $4.34\times 10^{-04} \pm 0.06 \times 10^{-04}$ S/cm (Figure 3.b). The results in Fig 3.b showed that by increasing the concentration of conductive microgels, the conductivity of the engineered composite hydrogel increased consistently. Concentration of conductive microgels could be tuned to provide a conductivity range up to $4.34\times 10^{-04} \pm 0.06 \times 10^{-04}$ S/cm and higher if more conductive microgels were incorporated to the backbone of the biopolymer. Studies have demonstrated the conductive nature of many tissues such as cardiac, lung, liver, nerve, chondrocytes, skeletal muscle all have a range overlapping in the 10^{-04} S/cm values (58-60), where the engineered conductive microgel system can be applied for promoting

tissue formation or conductive patches for the aforementioned tissue engineering applications.

Furthermore, the potential of the conductive microgels for excitable tissue constructs was evaluated to restore the propagation of electrical stimuli across severed skeletal muscle tissues ex vivo. Briefly, the conductive microgels at 50 wt% was selected and mixed with 10 wt% porcine GelMA to form the conductive composite hydrogel. Then after euthanatizing female Wistar rats, the rectus abdominis muscle of the rats were removed and placed 1-2 mm apart where the gap between the two pieces of tissue was filled with the conductive composite hydrogel, photocrosslinked for 4 minutes to apply pulsed direct current test runs (Figure 2.c). The results demonstrate a significantly lower excitation threshold where the muscle tissues joined together with the conductive composite hydrogel compared to pure GelMA controls (Figure 2.d). The result showed a 3-fold increase in the excitation threshold voltage of 4±1.73V for the 50 wt% microgel composition compared to 12.07±2.0V GelMA control. This result was in correlation with previous studies where severed ex vivo skeletal muscle tissues where restored with electroconductive hydrogels including Bio-IL/GelMA (30), PEDOT:PSS/GelMA (61), and GO/MeTro (62) hydrogels. The outcome of the threshold voltage for muscular stimulation demonstrated that the conductive microgels can be used to restore functional tissue integrity of tissues where electrophysiological communication can be received and transmitted from interrupted living tissues.

It was anticipated that the conductivity increases with the increase in conductive microgel concentration. The variation in conductivity shown in Figure 3.b increased and reached conductivity values above 10^{-04} S/cm past microgel concentration of 30 wt%, which we define as the microgel percolation threshold. The microgel distribution shown in Figure 2.a showed clearly past the critical concentration of 30 wt%, there was a large overlap of microgel-microgel

interactions. The mechanism of the conductivity in which the conductive microgels in the composite interacted with the living tissue can be through available carboxyl and amine functional groups on the tissue surface (63). The negatively charged carboxylate, and the positively charged amine groups on the tissue forms a spatial electron density featured pictorially in a red with the positively charged quaternary nitrogen of the choline. These dipole-dipole interactions mediated by Coulomb attractions are responsible for the ionic conductance responsible for restoring the electrophysiological communication of the severed tissue.

3.4 Printability of the engineered composite conductive hydrogel:

One of the main aims in tissue engineering is the fabrication of hydrogels and scaffolds with controlled architectures. In 3D bioprinting, bioinks composed of biological materials, biochemicals, and living cells are used to precisely form 3D structures (35). One of the main strategies employed for engineering these 3D structures is the extrusion based bioprinting where the bioinks are printed based on the designed architecture and shapes (5, 35, 64, 65). GelMA was selected as the base polymer for the development of an electroconductive bioink since GelMA mimics the ECM for maintaining cell viability and inducing desired cellular responses (66-69). One important aspect to create a 3D printed construct through extrusion based bioprinting is the viscosity of the bioink. The viscosity of GelMA prepolymer can be adjusted through parameters such as the polymer concentration and the temperature (67). In order to achieve suitable shape fidelity, the concentration of GelMA solution must be elevated to more than 30 wt%, which is detrimental to cell viability and cell bioactivity (68). In addition, performing printing at low temperature close to 0 °C can decrease the concentration of GelMA and the viscosity increases by the lowered temperature to achieve shape fidelity, however, lowering the temperature can result in filaments twisting, discontinuity of bioink, nozzle blockage and leads to cell damage (70).

These limitations have been assessed and resolved through using a freeform reversible embedding of suspended hydrogels (FRESH), a gel-in-gel printing approach where the bioink is directly extruded into a secondary support hydrogel, improving the shape fidelity while allowing the print of taller and more complex structures (5, 38, 41, 71-78). One of the main and common support bath hydrogels used for 3D bioprinting is the commercially available Carbopol, which is compatible with a wide range of bioinks used to print diverse multicellular structures (5, 41, 72, 75, 79, 80).

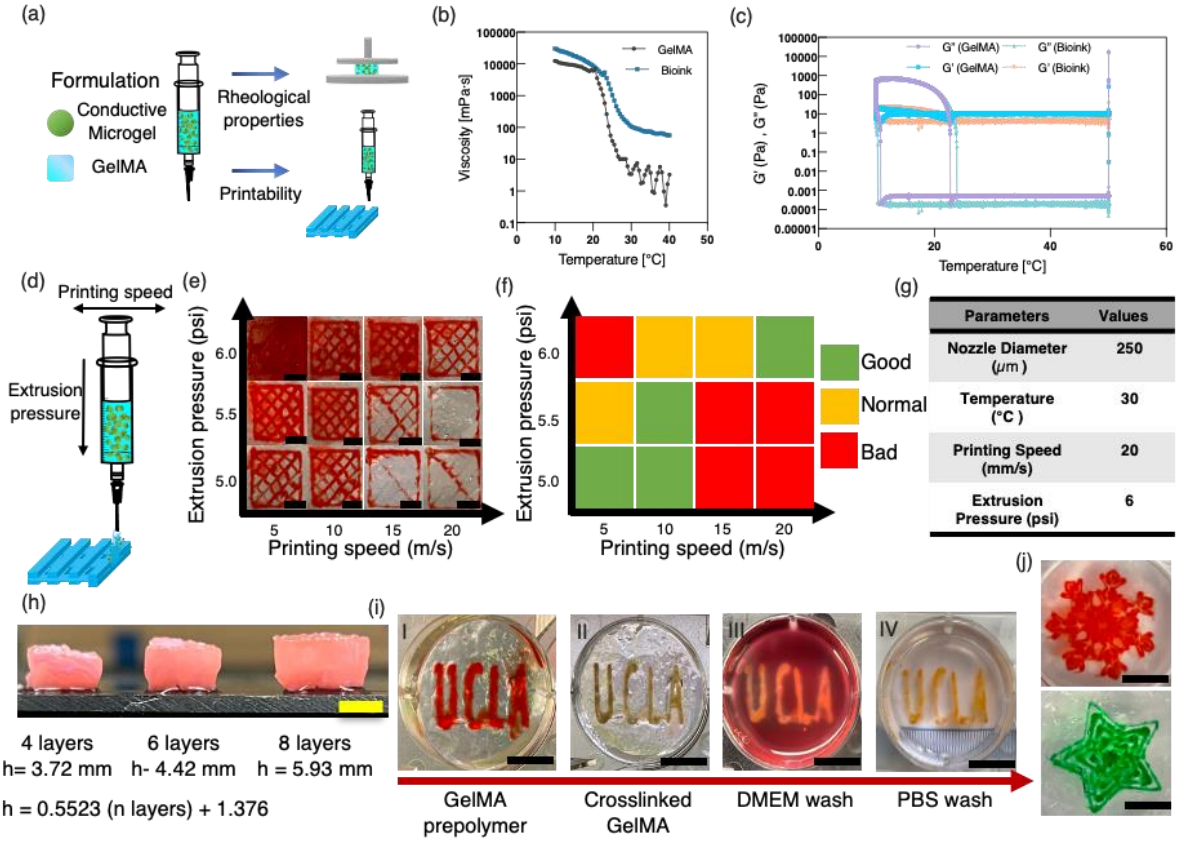

Figure 4: 3D printing optimization and characterization of the conductive composite hydrogel. A) Schematic of the bioink formulation and characterizations for 3D bioprinting. B) Viscosity of conductive composite hydrogel and GelMA as a function of temperature at the shear rate 50 s^{-1}. C) Storage modulus and loss modulus of the bioink as a function of temperature. D) Schematic of the optimization parameters, the printing speed, and extrusion pressure. E) A lattice-shaped

structure to optimize the printing speed and extrusion pressure of the conductive composite hydrogel (scale bar: 5 mm). F) Qualitative representative of the printing speed and extrusion pressure optimization. G) Optimized printing parameter for the conductive composite hydrogel. H) Different printed layers constructed with a linear relationship among the number of layers and the heigh of the construct (scale bar: 500 mm). I) Washing step optimization and representation: I: the printed hydrogel in the Carbopol bath shown stable, II: the printed structure is crosslinked with LED light for 4 minutes, III, IV: then washed with DMEM and PBS until the printed structure is free of the Carbopol support bath (scale bar: 1 cm). J) Various printed complex shapes (from top to bottom: a snowflake and a star) (scale bar: 1 cm).

In this work, we analyzed the bioink composite hydrogel by evaluating the rheological properties and printability characteristics (Figure 4.a). The injectability and thermo responsive behavior of the composite bioink was evaluated by the viscosity profile of GelMA and bioink in terms of temperature. The viscosity profile of the bioink and GelMA (control) was measured over the temperature range of 10 °C to 40 °C. The bioink containing microgels showed an increased viscosity as compared to GelMA (Figure 4.b). This is valuable since the bioink integrity can be maintained, making it stable for bioprinting. The variation of the storage modulus (G') and the loss modulus (G") over temperature range of 10 °C to 50 °C was monitored to select the extrusion head temperature. It was demonstrated that both samples were at their sol state at the printing temperature of 30 °C since the storage modulus (G') over the loss modulus (G") was significantly higher (Figure 4.c). Hence, the printability of the hydrogels was analyzed by setting the temperature of the support bath and syringe holder to 30 °C by adjusting the printing speed and extrusion pressure to evaluate the printed structure (Figure 4.d).

The extrusion pressure and printing speed were optimized to achieve optimal printing time

and shape fidelity (Figure 4.e) and then qualitatively assessed the printability categorized as good, normal, and bad (Figure 4.f). The final printing condition was selected to be at 6 psi and 20 mm/s (Figure 4.g). At these conditions the bioink smoothly exited the nozzle smoothly without forming any blockage and the resulting constructs were then crosslinked using visible light for 4 minutes. The stable hydrogels were printed in a multi-layered construct demonstrating that high aspect ratio structures can be printed (Figure 4.h). The printed layers were constructed at 4, 6, and 8 corresponding to 3.72, 4.42, and 5.93 mm, respectively, showing a linear trend line with the rms value of 0.95. Moreover, the printed photopolymerized constructs could be removed from the Carbopol support bath through a dilution of the medium as the washing step, where the structures were washed with DMEM and DPBS multiple times and then released from the Carbopol and placed in a DPBS solution (Figure 4.i). It was also demonstrated that complex architectures can be designed and printed and a snowflake with many curves were printed to represent this phenomenon (Figure 4.j). This characterization showed that the conductive microgels were stable in the bioink and printable with good shape fidelity and high aspect ratio as well as good resolution for forming complex geometries.

3.5 *In vitro* 2D/3D cell biocompatibility of the engineered conductive hydrogel:

One of the main challenges in the development of electroactive hydrogels for tissue engineering is to achieve not only applicable conductivity, but also not compromising the biocompatibility. The cytocompatibility of the conductive composite hydrogels was evaluated using different cell types. Initially mouse fibroblast cells were used then after the cytocompatibility evaluation, C2C12 myoblast cells were used for further evaluation. C2C12 myoblast cells have been shown to be sensitive to electrical stimulations for muscle development and differentiation (61, 81, 82).

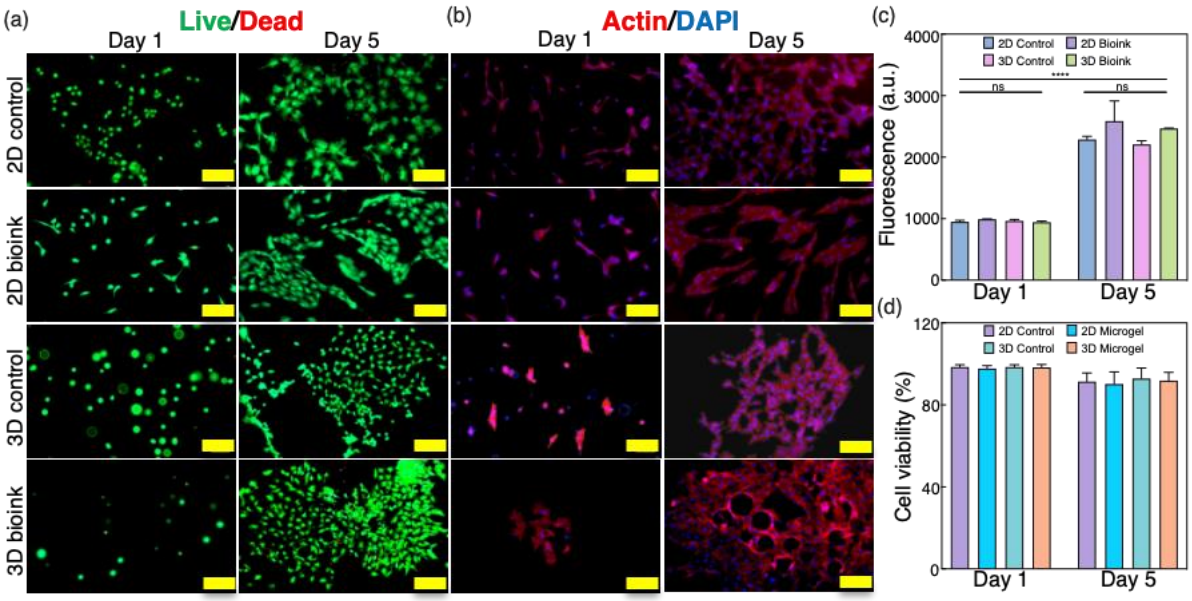

Figure 5: *In vitro* 2D and 3D encapsulation of C2C12 muscle cells in the composite hydrogels. A) Representative images from Live/Dead stained GelMA as the control and conductive composite hydrogel as the bioink post seeding and encapsulation at days 1, and 5. B) Representative images from Actin/DAPI stained GelMA as the control and conductive composite hydrogel as the bioink post seeding and encapsulation at days 1, and 5. C) Quantification of cell proliferation post days 1, 3, and 5. D) Quantification of cell viability post days 1, and 5 (Scale bar:100 μm) Error bars indicate standard error of the means, asterisks mark significance levels of $p < 0.05$ (*), $p < 0.01$ (**), $p < 0.001$ (***), and $p < 0.0001$ (****).

The cell viability was evaluated using a commercially live/dead assay where in the 2D cell seeding case cells were grown on the surface of GelMA (control) and the conductive composite hydrogels, and in the 3D cell encapsulation, cells were mixed with the precursor GelMA (control), and the conductive composite hydrogels then crosslinked and grown over the period of 5 days (Figure 5.a). Moreover, cell attachment and spreading on both GelMA (control) and the conductive

composite hydrogels were evaluated using F-actin/DAPI immunofluorescent staining (Figure 5.b), and the metabolic activities of the cells were studied using a commercially available PrestoBlue assay (Figure 5.c) over the period of 5 days. The viability of the cells seeded on the surface hydrogel and encapsulated in the hydrogel was not affected significantly by the incorporation of the conductive microgels (Figure 5.a). As shown in Figure 5.d, the viability of the cells seeded and 3D encapsulated in the control and conductive composite hydrogel did not exhibit any significant differences. The cells in duration of the study showed good attachment and was spread and elongated as shown by the F-actin/DAPI staining (Figure 5.b). There were also no significant differences in the attachment and spreading of the cells cultured on the GelMA and the conductive composite hydrogel (Figure 5.b). Furthermore, the metabolic activity of the cells in both culture condition (2D and 3D) increased consistently throughout the duration of the study for both GelMA and the conductive composite hydrogel (Figure 5.c). The addition of the conductive microgel to the GelMA polymer backbone did not affect the cell viability and supported cellular attachment and proliferation.

3.6 *In vitro* characterization of the 3D bioprinted conductive hydrogel:

In order to show that cell viability, attachment, spreading, and metabolic activity did not compromise during the printing process, C2C12 myoblast cells were encapsulated in the conductive composite hydrogel. The viability of the bioink was then investigated using the commercially live/dead assay over the period of 5 days (Figure 6.a). The cell attachment and spreading were evaluated using F-actin/DAPI immunofluorescent staining (Figure 6.b), and the metabolic activity of the cells were studied using a commercially available PrestoBlue assay did not affect during the extrusion process (Figure 6.b). Moreover, the metabolic activity of the bioprinted cells increased steadily over the period of 5 days culture. The effect of the extrusion

process on the cell viability, attachment, spreading, metabolic activity proved that the bioink and optimized printing set-up can be used for tissue engineering and tissue regeneration.

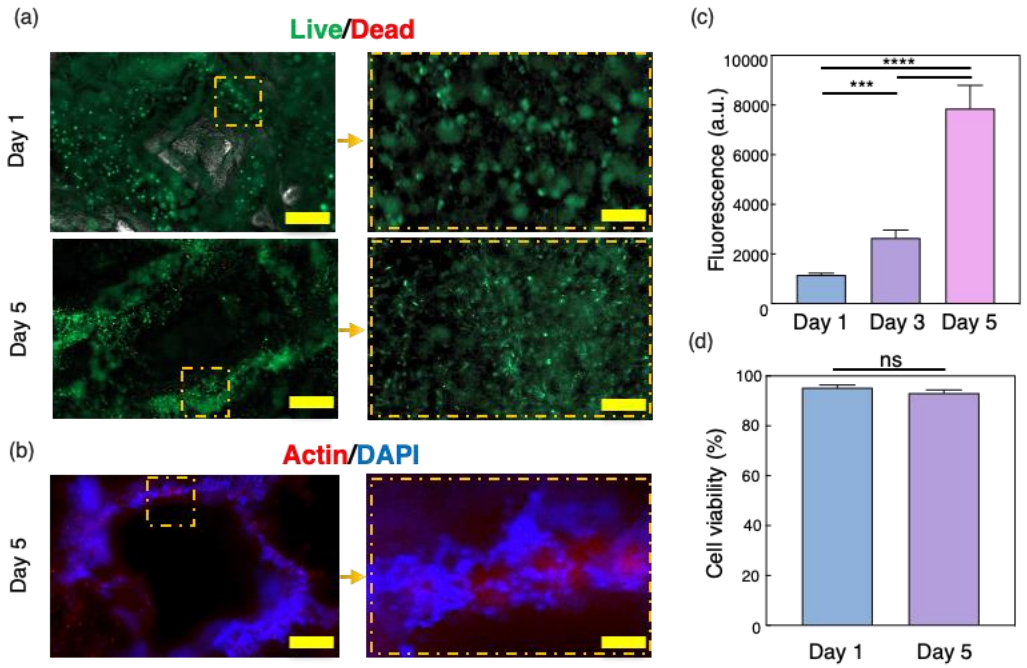

Figure 6: *In vitro* biocompatibility analysis of the printed cell-laden bioink. A) Representative images from Live/Dead stained conductive bioink post days 1, and 5 (scale bars from left to right: 500 µm and 100 µm). B) Representative image from Actin/DAPI stained samples post day 5 (scale bars from left to right: 500 µm and 100 µm). C) Quantification of cell proliferation post days 1, 3, and 5. D) Quantification of cell viability post Day 1, and 5. Error bars indicate standard error of the means, asterisks mark significance levels of $p < 0.05$ (*), $p < 0.01$ (**), $p < 0.001$ (***), and $p < 0.0001$ (****).

3.7 *In vivo* biocompatibility of the engineered conductive hydrogel:

A key characteristic for hydrogel implantation is its biodegradability. Most of the conventional conductive materials lack the proper biocompatibility and biodegradability *in vivo* that can result in body's immune response leading to inflammation (30). In this work, the *in vivo* biodegradation and immunogenicity profile were investigated through hydrogel implantation subcutaneously in rats. The *in vivo* samples were explanted at days 7, and 28 post-implantations, which revealed a sustained biodegradation throughout the duration of the experiment (Figure 7.a). Both the control (GelMA) and the conductive microgel composite hydrogel were degraded over time through enzymatic degradation. This was also visually verified and showed with tissue infiltration within the hydrogel (Figure 7.b).

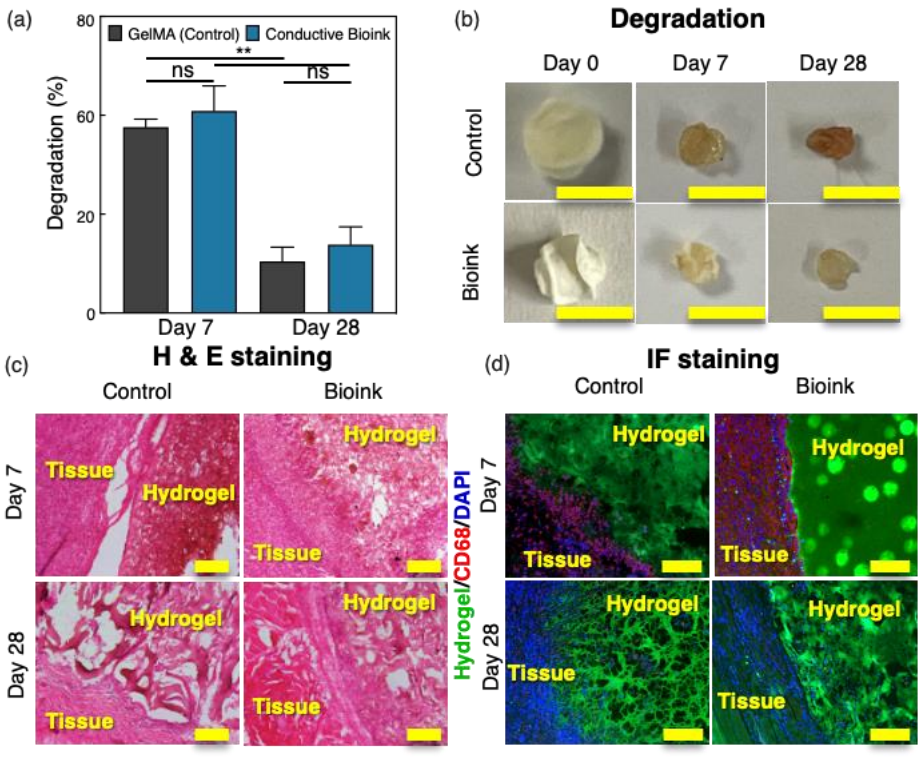

Figure 7: *In vivo* biodegradation and biocompatibility of the conductive composite hydrogel at 50 wt% microgel concentration and GelMA (control). A) Evaluation of the *in vivo* degradation based

on weight loss of conductive composite hydrogel and GelMA (control) GelMA/Bio-IL on days 0, 7, and 28 post implantations. B) Representative images of the conductive composite hydrogels and GelMA at 0, 7, and 28 days after implantation (scale bar: 5 mm). C) Hematoxylin and eosin (H&E) staining of explanted conductive composite hydrogel and GelMA post day 7 and day 28 (scale bar: 200 μm). D) Fluorescent immunohistochemical analysis of subcutaneously implanted conductive composite hydrogel and GelMA post day 7, and day 28 (scale bar: 200 μm), with no significant macrophage (CD68) presence at day 28. The green, red, and blue colors in represent the hydrogels, the immune cells, and the cell nuclei (DAPI).

The implanted hydrogel did not degrade completely in the duration of the study; however, studies have shown there are matrix metalloproteinase (MMP) sensitive degradation motifs available on GelMA based hydrogels that can facilitate the complete biodegradation of the GelMA biomaterial-based system (83, 84). This biodegradation permits sustained ingrowth of cells leading to eventual replacement of the implanted hydrogel 28 (Figure 7.d). These results demonstrated that the conductive composite hydrogel is with regenerated autologous tissue. The histological assessment of the explanted samples showed ingrowth of non-inflammatory tissues (Figure 7.c). This was confirmed by immunofluorescence analysis of the explanted samples using the expression of CD68 antigen, it was shown that macrophage response was elicited at day 7; however, this response was significantly reduced by day biodegradable and shows minimal inflammatory responses *in vivo*.

4 Conclusion:

In this work, a new strategy was developed to prepare conductive hydrogel using choline as the ionic precursor of conductivity. The choline was incorporated in a microgel system, which was fabricated using step-emulsifier microfluidics. The conductive choline-based microgels did not affect the mechanical properties of the backbone GelMA hydrogel significantly. This allows to fully take advantage of the versatility of the hydrogel matrix as a highly tunable backbone that can match properties of different electroactive tissue constructs such as stiffness and elasticity. The conductivity of the composite hydrogel was tunable based on the conductive microgels encapsulated in the backbone hydrogel, and conductivity values matching electroconductive tissue were achieved using this system. The threshold voltage also showed that the conductive composite hydrogel has the ability to restore electrophysiological communication that is necessary to restore functional tissue integrity of damaged electroconductive tissue. It is anticipated that by increasing the conductive microgel concentration, higher conductivity ranges can also be achieved; however, a systematic study is needed to confer changes in the mechanical properties of the backbone polymer. As a proof of concept, the injectability and printability of the composite hydrogel were analyzed as a viable method of bioprinting. This allows us to fully take advantage of the versatility of the hydrogel matrix as a highly tunable scaffold material and cell carrier, facilitating the formation of a complex tissue engineering construct with a conductivity function that is beyond its nature. The rheological analysis demonstrated the conductive bioink could be printed at higher than room temperature while achieving structural fidelity with a high aspect ratio and complex geometries using the FRESH method. The conductive composite hydrogel support cells viability and proliferation as well as spreading with increased metabolic activity. The extrusion of the bioink did not affect the abovementioned *in vitro* evaluation and showed the conductive composite

hydrogel can be used as a promising bioink for electroconductive tissue engineering. The composite hydrogel showed minimal inflammatory responses *in vivo* when implanted subcutaneously in rats. Taken together, the conductive choline-based microgels demonstrated the potential as an electroconductive hydrogel and bioprinting complex tissues that could ultimately be used for electroconductive tissue regeneration.

References:

1. S. Giwa *et al.*, The promise of organ and tissue preservation to transform medicine. *Nature biotechnology* **35**, 530-542 (2017).

2. H. Nekounam *et al.*, Electroconductive Scaffolds for Tissue Regeneration: Current opportunities, pitfalls, and potential solutions. *Materials Research Bulletin* **134**, 111083 (2021).

3. S. Kühn *et al.*, Cell-Instructive Multiphasic Gel-in-Gel Materials. *Advanced Functional Materials* **30**, 1908857 (2020).

4. E. Mostafavi *et al.*, Electroconductive nanobiomaterials for tissue engineering and regenerative medicine. *Bioelectricity* **2**, 120-149 (2020).

5. A. R. Spencer *et al.*, Bioprinting of a cell-laden conductive hydrogel composite. *ACS applied materials & interfaces* **11**, 30518-30533 (2019).

6. B. W. Walker *et al.*, Engineering a naturally-derived adhesive and conductive cardiopatch. *Biomaterials* **207**, 89-101 (2019).

7. B. W. Walker *et al.*, Rational design of microfabricated electroconductive hydrogels for biomedical applications. *Progress in polymer science* **92**, 135-157 (2019).

8. J. Xu, Y.-L. Tsai, S.-h. Hsu, Design strategies of conductive hydrogel for biomedical applications. *Molecules* **25**, 5296 (2020).

9. D. Gan *et al.*, Mussel-inspired redox-active and hydrophilic conductive polymer nanoparticles for adhesive hydrogel bioelectronics. *Nano-micro letters* **12**, 1-16 (2020).

10. N. Dubey, C. S. Kushwaha, S. Shukla, A review on electrically conducting polymer bionanocomposites for biomedical and other applications. *International Journal of Polymeric Materials and Polymeric Biomaterials* **69**, 709-727 (2020).

11. M. Song *et al.*, Constructing stimuli-free self-healing, robust and ultrasensitive biocompatible hydrogel sensors with conductive cellulose nanocrystals. *Chemical Engineering Journal* **398**, 125547 (2020).

12. S. Wang *et al.*, Fabrication of polypyrrole-grafted gelatin-based hydrogel with conductive, self-healing, and injectable properties. *ACS Applied Polymer Materials* **2**, 3016-3023 (2020).

13. K. Zhu *et al.*, Gold nanocomposite bioink for printing 3D cardiac constructs. *Advanced functional materials* **27**, 1605352 (2017).

14. Y. J. Lee, E.-Y. Ahn, Y. Park, Shape-dependent cytotoxicity and cellular uptake of gold nanoparticles synthesized using green tea extract. *Nanoscale research letters* **14**, 1-14 (2019).

15. S. J. Soenen *et al.*, Cytotoxic effects of gold nanoparticles: a multiparametric study. *ACS nano* **6**, 5767-5783 (2012).

16. S.-M. Chuang *et al.*, Extensive evaluations of the cytotoxic effects of gold nanoparticles. *Biochimica et Biophysica Acta (BBA)-General Subjects* **1830**, 4960-4973 (2013).

17. P. J. Chueh, R.-Y. Liang, Y.-H. Lee, Z.-M. Zeng, S.-M. Chuang, Differential cytotoxic effects of gold nanoparticles in different mammalian cell lines. *Journal of hazardous materials* **264**, 303-312 (2014).

18. A. C. Daly, L. Riley, T. Segura, J. A. Burdick, Hydrogel microparticles for biomedical applications. *Nature Reviews Materials* **5**, 20-43 (2020).

19. M. Karg *et al.*, Nanogels and microgels: From model colloids to applications, recent developments, and future trends. *Langmuir* **35**, 6231-6255 (2019).

20. C. L. Lin, W. Y. Chiu, Polypyrrole/poly (N-isopropylacrylamide-co-acrylic acid) thermosensitive and electrically conductive composite microgels. *Journal of Polymer Science Part A: Polymer Chemistry* **44**, 1648-1659 (2006).

21. Y.-B. Kim, J.-K. Choi, J.-A. Yu, J.-W. Hong, Synthesis and characterization of a non-aqueous conductive microgel coated with poly (aniline)–DBSA in a colloidal dispersion. *Synthetic metals* **131**, 79-85 (2002).

22. C. Zhang, C. Li, Y. Chen, Y. Zhang, Synthesis and catalysis of Ag nanoparticles trapped into temperature-sensitive and conductive polymers. *Journal of Materials Science* **49**, 6872-6882 (2014).

23. Y. Hu *et al.*, Preparation of large micron-sized monodisperse polystyrene/silver core–shell microspheres with compact shell structure and their electrical conductive and catalytic properties. *Rsc Advances* **5**, 58-67 (2015).

24. S. Shang, J. Liu, Y. He, P. Zhu, Smart conducting PNIPAM-co-AAc microgels with controllable phase transition and stimuli responsibility. *Materials Letters* **272**, 127862 (2020).

25. Y. Zhao *et al.*, Microgel-enhanced double network hydrogel electrode with high conductivity and stability for intrinsically stretchable and flexible all-gel-state supercapacitor. *ACS applied materials & interfaces* **10**, 19323-19330 (2018).

26. V. R. Feig *et al.*, Conducting Polymer-Based Granular Hydrogels for Injectable 3D Cell Scaffolds. *Advanced Materials Technologies* **6**, 2100162 (2021).

27. M. Shin, K. H. Song, J. C. Burrell, D. K. Cullen, J. A. Burdick, Injectable and conductive granular hydrogels for 3D printing and electroactive tissue support. *Advanced Science* **6**, 1901229 (2019).

28. R. Klein *et al.*, Biodegradability and cytotoxicity of choline soaps on human cell lines: effects of chain length and the cation. *RSC advances* **3**, 23347-23354 (2013).

29. I. Noshadi *et al.*, Engineering biodegradable and biocompatible bio-ionic liquid conjugated hydrogels with tunable conductivity and mechanical properties. *Scientific reports* **7**, 1-18 (2017).

30. A. Le Donne, E. Bodo, Cholinium amino acid-based ionic liquids. *Biophysical reviews* **13**, 147-160 (2021).

31. J. Zhou, S. Vijayavenkataraman, 3D-printable conductive materials for tissue engineering and biomedical applications. *Bioprinting* **24**, e00166 (2021).

32. V. Krishnadoss *et al.*, Bioionic liquid conjugation as universal approach to engineer hemostatic bioadhesives. *ACS applied materials & interfaces* **11**, 38373-38384 (2019).

33. E. E. Tanner *et al.*, The influence of water on choline-based ionic liquids. *ACS Biomaterials Science & Engineering* **5**, 3645-3653 (2019).

34. S. V. Murphy, A. Atala, 3D bioprinting of tissues and organs. *Nature biotechnology* **32**, 773-785 (2014).

35. R. Jamee, Y. Araf, I. B. Naser, S. K. Promon, The promising rise of bioprinting in revolutionalizing medical science: Advances and possibilities. *Regenerative Therapy* **18**, 133-145 (2021).

36. J. Park *et al.*, Cell-laden 3D bioprinting hydrogel matrix depending on different compositions for soft tissue engineering: Characterization and evaluation. *Materials Science and Engineering: C* **71**, 678-684 (2017).

37. D. J. Shiwarski, A. R. Hudson, J. W. Tashman, A. W. Feinberg, Emergence of FRESH 3D printing as a platform for advanced tissue biofabrication. *APL bioengineering* **5**, 010904 (2021).

38. T. J. Hinton *et al.*, Three-dimensional printing of complex biological structures by freeform reversible embedding of suspended hydrogels. *Science advances* **1**, e1500758 (2015).

39. K. Yue *et al.*, Synthesis, properties, and biomedical applications of gelatin methacryloyl (GelMA) hydrogels. *Biomaterials* **73**, 254-271 (2015).

40. J. M. de Rutte, J. Koh, D. Di Carlo, Scalable high-throughput production of modular microgels for in situ assembly of microporous tissue scaffolds. *Advanced Functional*

Materials **29**, 1900071 (2019).

41. S. Lee *et al.*, Human-recombinant-Elastin-based bioinks for 3D bioprinting of vascularized soft tissues. *Advanced Materials* **32**, 2003915 (2020).

42. S. Baghdasarian *et al.*, Engineering a naturally derived hemostatic sealant for sealing internal organs. *Materials Today Bio*, 100199 (2021).

43. W. Leong, T. T. Lau, D.-A. Wang, A temperature-cured dissolvable gelatin microsphere-based cell carrier for chondrocyte delivery in a hydrogel scaffolding system. *Acta biomaterialia* **9**, 6459-6467 (2013).

44. M. E. Helgeson, S. C. Chapin, P. S. Doyle, Hydrogel microparticles from lithographic processes: Novel materials for fundamental and applied colloid science. *Current opinion in colloid & interface science* **16**, 106-117 (2011).

45. A. Í. Morais *et al.*, Fabrication of polymeric microparticles by electrospray: the impact of experimental parameters. *Journal of functional biomaterials* **11**, 4 (2020).

46. V. G. Muir, T. H. Qazi, J. Shan, J. r. Groll, J. A. Burdick, Influence of microgel fabrication technique on granular hydrogel properties. *ACS Biomaterials Science & Engineering* **7**, 4269-4281 (2021).

47. S. L. Anna, N. Bontoux, H. A. Stone, Formation of dispersions using "flow focusing" in microchannels. *Applied physics letters* **82**, 364-366 (2003).

48. N. Zoratto *et al.*, In situ forming microporous gelatin methacryloyl hydrogel scaffolds from thermostable microgels for tissue engineering. *Bioengineering & Translational Medicine* **5**, e10180 (2020).

49. H. J. Yoon *et al.*, Cold water fish gelatin methacryloyl hydrogel for tissue engineering application. *PloS one* 11, e0163902 (2016).

50. Y. Atma, Synthesis and Application of Fish Gelatin for Hydrogels/Composite Hydrogels: A Review. *peptides* **22**, 23 (2021).

51. M. E. Chicurel, C. S. Chen, D. E. Ingber, Cellular control lies in the balance of forces. *Current opinion in cell biology* **10**, 232-239 (1998).

52. S. Jadoun, U. Riaz, V. Budhiraja, Biodegradable conducting polymeric materials for biomedical applications: A review. *Medical Devices & Sensors* **4**, e10141 (2021).

53. J. M. Gomes, S. S. Silva, R. L. Reis, Biocompatible ionic liquids: fundamental behaviours and applications. *Chemical Society Reviews* **48**, 4317-4335 (2019).

54. X. Liang *et al.*, Preparation of cellulose-based conductive hydrogels with ionic liquid.

Reactive and Functional polymers **86**, 1-6 (2015).

55. S. S. Robinson *et al.*, Integrated soft sensors and elastomeric actuators for tactile machines with kinesthetic sense. *Extreme Mechanics Letters* **5**, 47-53 (2015).

56. Y. Lu, R. Liu, X.-C. Hang, D. J. Young, Biocompatible, flexible and conductive polymers prepared by biomass-derived ionic liquid treatment. *Polymer Chemistry* **12**, 2115-2121 (2021).

57. P. Zarrintaj *et al.*, Agarose-based biomaterials for tissue engineering. *Carbohydrate polymers* **187**, 66-84 (2018).

58. C. Gabriel, A. Peyman, E. H. Grant, Electrical conductivity of tissue at frequencies below 1 MHz. *Physics in medicine & biology* **54**, 4863 (2009).

59. T. H. Qazi *et al.*, Development and characterization of novel electrically conductive PANI–PGS composites for cardiac tissue engineering applications. *Acta biomaterialia* **10**, 2434-2445 (2014).

60. A. R. Spencer *et al.*, Electroconductive gelatin methacryloyl-PEDOT: PSS composite hydrogels: Design, synthesis, and properties. *ACS biomaterials science & engineering* **4**, 1558-1567 (2018).

61. N. Annabi *et al.*, Highly elastic and conductive human-based protein hybrid hydrogels. *Advanced Materials* **28**, 40-49 (2016).

62. X. Pei, J. Wang, Y. Cong, J. Fu, Recent progress in polymer hydrogel bioadhesives. *Journal of Polymer Science* **59**, 1312-1337 (2021).

63. N. Betancourt, X. Chen, Review of extrusion-based multi-material bioprinting processes. *Bioprinting*, e00189 (2022).

64. I. T. Ozbolat, M. Hospodiuk, Current advances and future perspectives in extrusion-based bioprinting. *Biomaterials* **76**, 321-343 (2016).

65. Z. Gu, J. Fu, H. Lin, Y. He, Development of 3D bioprinting: From printing methods to biomedical applications. *Asian Journal of Pharmaceutical Sciences* **15**, 529-557 (2020).

66. I. Pepelanova, K. Kruppa, T. Scheper, A. Lavrentieva, Gelatin-methacryloyl (GelMA) hydrogels with defined degree of functionalization as a versatile toolkit for 3D cell culture and extrusion bioprinting. *Bioengineering* **5**, 55 (2018).

67. G. Ying, N. Jiang, C. Yu, Y. S. Zhang, Three-dimensional bioprinting of gelatin methacryloyl (GelMA). *Bio-Design and Manufacturing* **1**, 215-224 (2018).

68. J. Yin, M. Yan, Y. Wang, J. Fu, H. Suo, 3D bioprinting of low-concentration cell-laden

gelatin methacrylate (GelMA) bioinks with a two-step cross-linking strategy. *ACS applied materials & interfaces* **10**, 6849-6857 (2018).

69. A. Mostafavi *et al.*, Colloidal multiscale porous adhesive (bio) inks facilitate scaffold integration. *Applied Physics Reviews* **8**, 041415 (2021).

70. Y. Gu *et al.*, Reversible physical crosslinking strategy with optimal temperature for 3D bioprinting of human chondrocyte-laden gelatin methacryloyl bioink. *Journal of biomaterials applications* **33**, 609-618 (2018).

71. A. M. Compaan, K. Song, W. Chai, Y. Huang, Cross-linkable microgel composite matrix bath for embedded bioprinting of perfusable tissue constructs and sculpting of solid objects. *ACS Applied Materials & Interfaces* **12**, 7855-7868 (2020).

72. T. Bhattacharjee *et al.*, Writing in the granular gel medium. *Science advances* **1**, e1500655 (2015).

73. W. Cheng, J. Zhang, J. Liu, Z. Yu, Granular hydrogels for 3D bioprinting applications. *View* **1**, 20200060 (2020).

74. A. McCormack, C. B. Highley, N. R. Leslie, F. P. Melchels, 3D printing in suspension baths: keeping the promises of bioprinting afloat. *Trends in Biotechnology* **38**, 584-593 (2020).

75. Y. Zhang *et al.*, 3D printed collagen structures at low concentrations supported by jammed microgels. *Bioprinting* **21**, e00121 (2021).

76. T. G. Molley *et al.*, Heterotypic tumor models through freeform printing into photostabilized granular microgels. *Biomaterials Science* **9**, 4496-4509 (2021).

77. Z.-T. Xie, D.-H. Kang, M. Matsusaki, Resolution of 3D bioprinting inside bulk gel and granular gel baths. *Soft Matter* **17**, 8769-8785 (2021).

78. Q. Feng, D. Li, Q. Li, X. Cao, H. Dong, Microgel assembly: Fabrication, characteristics and application in tissue engineering and regenerative medicine. *Bioactive materials* **9**, 105-119 (2022).

79. T. Bhattacharjee *et al.*, Liquid-like solids support cells in 3D. *ACS Biomaterials Science & Engineering* **2**, 1787-1795 (2016).

80. Y. Jin, A. Compaan, T. Bhattacharjee, Y. Huang, Granular gel support-enabled extrusion of three-dimensional alginate and cellular structures. *Biofabrication* **8**, 025016 (2016).

81. L. Li, J. Ge, B. Guo, P. X. Ma, In situ forming biodegradable electroactive hydrogels. *Polymer Chemistry* **5**, 2880-2890 (2014).

82. R. Breukers *et al.*, Creating conductive structures for cell growth: Growth and alignment of myogenic cell types on polythiophenes. *Journal of Biomedical Materials Research Part A* **95**, 256-268 (2010).

83. S. T. Koshy, T. C. Ferrante, S. A. Lewin, D. J. Mooney, Injectable, porous, and cell-responsive gelatin cryogels. *Biomaterials* **35**, 2477-2487 (2014).

84. Y. C. Chen *et al.*, Functional human vascular network generated in photocrosslinkable gelatin methacrylate hydrogels. *Advanced functional materials* **22**, 2027-2039 (2012).